УДК 551.465.78:627.222.23

© *В. А. Рябченко*[1], *И. О. Леонтьев*[1], *Д. В. Рябчук*[2,3], *А. Ю. Сергеев*[2], *А. Ю. Дворников*[1], *С. Д. Мартьянов*[1], *В. А. Жамойда*[2,3]
[1]Институт океанологии им. П.П. Ширшова РАН, г. Москва
[2]Всероссийский научно-исследовательский геологический институт им. А. П. Карпинского (ВСЕГЕИ), г. Санкт-Петербург
[3]Санкт-Петербургский государственный университет, Институт наук о Земле, г. Санкт-Петербург
vla-ryabchenko@yandex.ru

МЕРЫ ПО СМЯГЧЕНИЮ ПОСЛЕДСТВИЙ БЕРЕГОВОЙ ЭРОЗИИ НА ПОБЕРЕЖЬЕ ОСТРОВА КОТЛИН В ФИНСКОМ ЗАЛИВЕ, БАЛТИЙСКОЕ МОРЕ

Статья поступила в редакцию 30.01.2018, после доработки 04.04.2018.

Интенсивная эрозия берегов вблизи острова Котлин в Финском заливе, наблюдаемая в последние 70 лет, может привести к полному исчезновению песчаных пляжей в западной части о. Котлин в ближайшем будущем. В статье оценивается интенсивность береговой эрозии в западной части о. Котлин и предлагается метод искусственной подсыпки, обеспечивающий сохранение песчаных пляжей. Геологические исследования выявили следующие особенности прибрежной зоны моря и берега в западной части о. Котлин: 1) значительный дефицит донных осадков; 2) небольшая (около 30 см) толщина активного песчаного слоя, 3) преобладание узких (10—15 м) песчаных пляжей и 4) низкий и плавный рельеф морского дна и берега. Параметры искусственного пляжа определяются из совместной модели, объединяющей модели циркуляции воды, ветровых волн и динамики осадков. Расчеты скорости течений и ветровых волн проводились с использованием трехмерной гидродинамической модели восточной части Финского залива и волновой модели SWAN, соответственно. Деформация побережья из-за штормовых нагонов была рассчитана на основе модели CROSS-P. Исходными данными были начальный профиль глубины, характеристики донных осадков, скорость ветра, изменения уровня воды и параметров волн во время шторма, его продолжительность. По заданным внешним воздействиям (атмосферный форсинг из модели HIRLAM, граничные условия на открытой водной границе из модели HIROMB, рельеф дна и пляжа в прибрежной зоне по результатам вышеуказанных геологических исследований) рассчитаны параметры профиля искусственного пляжа при максимальном штормовом нагоне, и оценен годовой объем песка, необходимый для сохранения искусственного пляжа.

Ключевые слова: Эрозия берегов, течения, ветровые волны, динамика осадков, моделирование, искусственный пляж, остров Котлин, Финский залив, Балтийское море.

V. A. Ryabchenko[1], *I. O. Leontyev*[1], *D. V. Ryabchuk*[2,3], *A. Yu. Sergeev*[2], *A. Yu. Dvornikov*[1], *S. D. Martyanov*[1], *V. A. Zhamoida*[2,3]
[1]Shirshov Institute of Oceanology, Russian Academy of Sciences; Moscow, Russia
[2]A. P. Karpinsky Russian Geological Research Institute (VSEGEI); St.-Petersburg, Russia
[3]St.-Petersburg State University, Institute of Earth Science; St.-Petersburg, Russia

MITIGATION MEASURES OF COASTAL EROSION ON THE KOTLIN ISLAND'S SHORES IN THE GULF OF FINLAND, THE BALTIC SEA

Received 30.01.2018, in final form 04.04.2018.

The intense erosion of shores of the Kotlin Island in the Gulf of Finland during the last 70 years can lead to the complete disappearance of sandy beaches of the western Kotlin Island in the near future. We assess the intensity of the

Ссылка для цитирования: *Рябченко В. А., Леонтьев И. О., Рябчук Д. В., Сергеев А. Ю., Дворников А. Ю., Мартьянов С. Д., Жамойда В. А.* Mitigation measures of coastal erosion on the Kotlin Island's shores in the Gulf of Finland, the Baltic Sea // Фундаментальная и прикладная гидрофизика. 2018. Т. 11, № 2. С. 36—50.

For citation: *Ryabchenko V. A., Leontyev I. O., Ryabchuk D. V., Sergeev A. Yu., Dvornikov A. Yu., Martyanov S. D., Zhamoida V. A.* Mitigation measures of coastal erosion on the Kotlin Island's shores in the Gulf of Finland, the Baltic Sea. *Fundamentalnaya i Prikladnaya Gidrofizika.* 2018, 11, 2, 36—50.

doi: 10.7868/S207366731802003X

coastal erosion of the western Kotlin Island and propose the method of artificial sand nourishment in order to maintain the sandy beaches. The geological near-shore and onshore surveys revealed the following features of the western Kotlin Island coastal zone: 1) significant sediment deficit; 2) small (about 30 cm) thickness of the active sand layer, 3) predominance of narrow (10—15 m) sand beaches and 4) low and smooth offshore and onshore topography. The parameters of artificial beaches are determined by coupling the models of water circulation, waves, and sediment dynamics. Calculations of currents and waves were performed using a three-dimensional hydrodynamic model of the eastern Gulf of Finland and the SWAN wave model, respectively. The coast deformation due to storms was calculated using the CROSS-P model. Initial data were the existing depth profile, sediment characteristics, wind properties, wave parameters, the height of storm surges, and the duration of a storm. The actual external forcing (atmospheric forcing from the HIRLAM model, open boundary conditions from the HIROMB model, and bathymetry and topography of the beach obtained from geological surveys) is given, the parameters of artificial beach profiles have been calculated to withstand the maximum storm surge, and the annual volume of sand necessary for the conservation of the artificial beaches has been estimated.

Key words: Coastal erosion, currents, wind waves, sediment dynamics, modelling, artificial beach, Kotlin Island, Gulf of Finland, Baltic Sea.

1. Introduction. In recent decades considerable progress has been made in the development of mathematical modelling of the coastal dynamics. Although the possibilities of morphodynamic forecasts are still limited, existing models already provide significant assistance in solving practical problems related, for example, to the assessment of longshore sediment transport, changes in the coastline [1, 2] and also to predictions of storm-induced bed deformations [3, 4].

The main motivation for the research in this paper was the retrospective analysis of the remote sensing data about the coastal zone of the western shores of the Kotlin Island (KI) in the eastern Gulf of Finland (GoF) (fig. 1, see an insert). This data set revealed the maximal erosion rates of 1.2—1.6 m/year during the last 76 years. The average rate of shoreline recession is about 0.25—0.5 m/year [5]. This process can lead to the complete disappearance of sandy beaches of the western KI in the nearest future.

The most adequate approach to the modelling of morphodynamical processes depends on the time scales considered. In this study the focus is on processes that occur on the typical time scale of single storms. These scales are at best resolved using so-called process-based models [6, 7]. They are able to simulate the local effects of waves and currents on the sand bottom and ultimately lead to acceptable estimates of sediment transport and associated changes in coastal morphology.

The purpose of this study is to assess the intensity of coastal erosion in the western part of the KI (fig. 2, see an insert) characterised by the great abrasion intensity and to propose realistic measures to maintain its sand beaches. We generalise this particular result towards proposing a method for assessing the impact of potentially dangerous geological processes in the coastal zone based on actual geological and geophysical information, modelling of circulation patterns in nearshore, waves and sediment dynamics, and recommendations how to combine these modelling efforts for practical purposes.

2. Methods

2.1. Geological and geophysical studies. To achieve our goals, we employ subsequently a cluster of different data sources and a hierarchy of numerical models (fig. 3).

Marine fieldwork was carried out by the A. P. Karpinsky Russian Geological Research Institute (VSEGEI) during summer 2016 on boards of research vessels (RVs). The nearshore zone was imaged using the side-scan sonar (CM2, C-MAX Ltd, UK) with a depth-dependent search swath of 75 m and a working acoustic frequency of 325 kHz. More than 400 km of side-scan images allowed compiling a full-coverage side-scan sonar mosaic of the seabed in the study area. Twenty kilometres of low-frequency acoustic seismic profiling was carried out using 0.2—5.0 kHz boomer sub-bottom profiler GEONT–HRP (Spectr-Geophysika Ltd., Russia) with a 0.4 m resolution. The signal penetration depth depends on geological properties and varied in the range of 20—25 m.

Geophysical profiling was accompanied by echo-sounding («HydroBoxTM», SYQWEST, USA). The interpretation of sonar data was supported by sediment sampling using a box-corer (44 sites) and underwater video observations (10 sites) using a video-ROV Super-Gnom (manufactured by P. P. Shirshov Institute of Oceanology, Russia) and further improved with high-definition camera GoPro™ HDHERO2.The positioning of devices was controlled using GPS systems Furuno 7000F, Garmin GPSMAP60 CSx, and Vector VS330. This data set was complemented by measurements of beach profiles in the nearshore areas along several

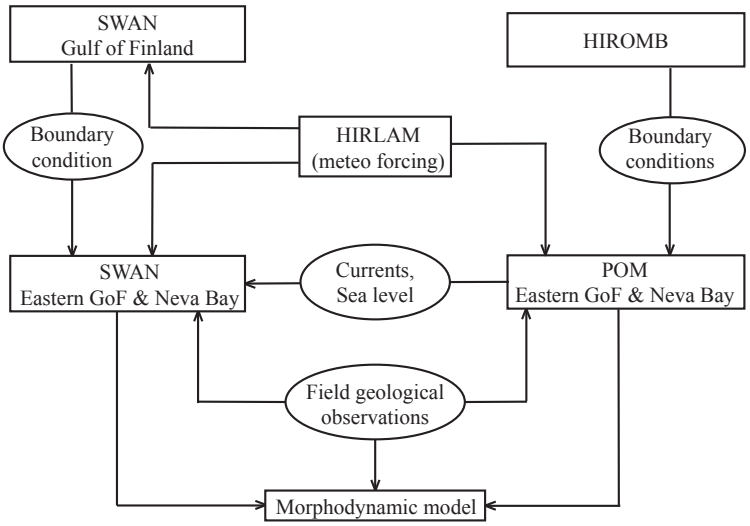

Fig. 3. General scheme of the interaction between models and data.

Рис. 3. Общая схема взаимодействия моделей и данных.

transects perpendicular to shoreline. The sand layer thickness was determined using shallow drilling in three sites (KDT-5–KDT-7).

The onshore geological research was focused on the observation of the intensity of coastal erosion and the identification of the local features of sub-surface geological structure (e.g. beach and dune structure, lamination, character of the inner boundaries, sand layer thickness, etc.). The ground-penetrating radar (GPR) surveys (the total length of transects about 1.5 km) were used to obtain continuous high-resolution subsurface images. The GPR setup included a digital Geophysical Survey Systems Inc. SIR-2000 GPR system with a 400 MHz monostatic antenna. The penetration depth of the signal was 5—7 m. The interpretation of radar data was supported by 10 boreholes (each about 2 m deep, 12 cm in diameter) drilled by STIHL BT 121.

Grain-size analyses of sediment samples were carried out and the main grain-size statistical parameters (mean diameter Md, Ma, So, A) were calculated [8] in the VSEGEI laboratory using laser diffractometer Microsizer 201A (VA Instal, Russia) and an analytical sieve shaker (AS 200 Retsch). The samples were separated into 21 grain-size classes.

2.2. Modelling of circulation and wind waves

Circulation model. Calculations of velocities of currents were performed using a three-dimensional hydrodynamic model of the eastern part of the GoF and the Neva Bay [9]. The model was verified via the calculation of the spreading of sewage from Saint Petersburg from the emission points in the Neva Bay in summer and winter conditions [9, 10] and during the simulation of storm surges in the situation when the Saint Petersburg Flood Protection Barrier (FPB) was operational [11]. The model is based on the three-dimensional Princeton Ocean Model (POM) [12] that uses the σ-coordinate in the vertical direction.

The model domain covers the eastern GoF including the Neva Bay and the vicinity of the FPB (fig. 2, *b*). Its eastern boundary (the estuary of the River Neva) is at the longitude 30º14'59"E and the western one at the longitude 29º08'08"E. The model uses a regular grid with a step of 100 m in the horizontal direction. The number of grid nodes in the *x*-direction (from west to east) is 600 and in the *y*-direction (from south to north) 400.The number of uniformly distributed σ-levels is 7. The maximum depth is 34.4 m and the minimum depth is 0.2 m. The FPB has six water gates and two ship gates. The model allows for opening and closing of these gates during the calculations.

Wind waves. The calculation of wave parameters was carried out using the wave model SWAN that is developed specifically for describing waves in shallow shelf and coastal areas with a complex bathymetry and geometry [13, 14]. This model was successfully used to simulate wind waves in the Neva Bay and the eastern GoF [15]. In this study the SWAN model was applied for the eastern GoF (fig. 2, *b*). The spatial resolution of the SWAN model (100 m) was the same as for the circulation model. When simulating waves in the study area it is extremely important to reproduce the properties of waves generated in the GoF and affecting the western

coast of the KI during strong western storms. To simulate such conditions at the open boundary, we performed SWAN model runs in advance for the entire GoF on a larger grid containing 720×310 nodes.

2.3. Modelling of sediment transport and morphodynamics

The modelling of sediment transport is based on the energetics approach [16—18]. The local volumetric cross-shore (axis x) and longshore (axis y) net sediment transport q_x and q_y ($m^3m^{-1}s^{-1}$) in the wave shoaling and the surf zones are determined by the following expressions:

$$q_x = q^0 - 2\beta\left|q^0\right|,\ q^0 = \mu\left\{\left[\frac{9\pi}{8}\frac{\varepsilon_b}{\tan\varphi}D_f + \varepsilon_s\frac{u_m}{w_g}\left(4D_f + D_{br}\right)\right]\frac{U_w + U_c}{u_m} + q_{BS}\cos\Theta\right\},$$

$$q_y = \mu\left\{\left[\frac{9\pi}{8}\frac{\varepsilon_b}{\tan\varphi}D_f + \varepsilon_s\frac{u_m}{w_g}\left(4D_f + D_{br}\right)\right]\frac{V_w + V_c}{u_m} + q_{BS}\sin\Theta\right\},\ \mu = \left[g(\rho_g - \rho)(1-\sigma)\right]^{-1},$$

where $\beta = -\partial h / \partial x$ is the bottom slope, h is the water depth (the z-axis is directed upwards and $h = 0$ correspond to the free surface), q^0 is the cross-shore net transportover a horizontal bed, g is gravity acceleration, ρ is the water density, ρ_g and σ are the density and porosity of solid grains, respectively, ε_b and ε_s are the bed-load and suspended-load transport efficiency coefficients, respectively, φ is the angle of repose, u_m is the amplitude of near-bed wave orbital velocities, w_g is the grain settling velocity in water, D_f is the energy dissipation rate due to bed friction, D_{br} is the additional dissipation rate near the bed due to wave breaking, U_w, U_c and V_w, V_c are the near-bed cross-shore and longshore mass transport velocities induced by waves (w) and currents (c), q_{BS} is the net transportdue to the burst of sediment suspension in the wave breaking region, and Θ is the angle of incidence of the wave relative to the normal to the coastline.

In the swash zone, a peak value of the cross-shore net sediment transport is determined by the relationships:

$$\hat{q}_{xR} = \mu K_R \rho u_R^3\left(\beta_{eq} - \overline{\beta}\right),\ u_R = \sqrt{2gR},$$

where K_R=0.005 is a scaling factor, u_R is the amplitude of run-up velocity, R is the height of wave run-up, $\overline{\beta}$ is the mean bed slope, and β_{eq} is the equilibrium beach slope depending on sediment grain size and wave parameters. See details in [4], [18—21].

The total net longshore sediment transport q_{total} is calculated by integrating the values of the local net transport at different depths q_y over the length l_* of the cross-shore coastal profile. The bulk longshore sediment transport Q is determined as the cumulative sediment volume transported through the cross-shore coastal profile for a given time interval with a duration of t_w:

$$q_{\text{total}} = \int_0^{l_*} q_y dx,\ Q = \int_0^{t_w} q_{\text{total}} dt.$$

Taking, for example, t_w=1 year we get the bulk annual sediment transport in cubic metres (m^3).

Storm-induced deformations of the coastal profile are computed from the equation of mass conservation:

$$\frac{\partial h}{\partial t} = \frac{\partial q_x}{\partial x},$$

where h is the local water depth and t is time. We employed the CROSS-P model that was previously successfully applied to the coasts of the eastern GoF [21, 22]. The set of input data for calculations are the depth profile $h(x)$, sediment characteristics (mean grain size, density, and porosity), wave parameters (height, period, angle of incidence), the height of the storm surge, wind speed, and storm duration. The equation of mass conservation is integrated with the time step Δt that matches the typical wave period and the spatial step Δx of the order of 1 m. At each time step the cross-shore distributions of the local wave parameters are computed. The sediment transport rates q_x and q_y are evaluated next. Based on the obtained values of q_x, the local changes to the bottom (expressed via the water depth) are calculated and the new depth profile $h(x)$ is determined.

If the local bottom slope exceeds a threshold limit ($\tan\varphi$ about 0.6), it is assumed that the sand will create a local avalanche. The model also reproduces the process of foredune overtopping during extreme surges. The swash-zone sediment transport rate depends on the relation $\Delta Z/R$, where ΔZ is the excess of the wave run-up R above the dune crest [4, 21].

The derived recommendations for beach protection are based on the model of an artificial beach developed under an extremely high storm surge [23]. The model allows estimating the amount of material necessary for the construction of the beach depending on the specified storm parameters, selected sediment size and desired width of the dry beach. Its description is given in Appendix 1. The stability of designed beaches is verified by modelling the impact of an extreme storm.

3. Geology and topography of the western coastal zone of the KI

3.1. Geology, topography and bathymetry of the coastal zone. The eastern GoF and KI are situated in the transition zone between the Baltic Shield and the East European Platform. Pre-Quaternary surface in the area of KI is represented by Vendian clays. According to results of onshore [24] and offshore [25] state geological surveys, the geological structure of KI and the adjacent nearshore bottom is controlled by glacial moraine elevation partly covered by Late Pleistocene clays. Sand accretion sediments formed during Holocene transgressions of the Baltic are widely spread onshore.

According to long-term high-resolution levellings in the 1970s–1990s in Russia, Finland and Estonia, the study area is characterised by tectonic uplift with the rate of 0.5—1.5 mm/year [26]. This process obviously impacts the intensity of coastal erosion. However, the relative sea level increased by 6—12 cm in Kronstadt according to measurements in 1945—2007 [27].

The geological and geophysical studies performed in 2016—2017 allowed compiling a detailed map of bottom sediment distribution for the nearshore of the study area (fig. 4, see an insert). The most important feature (from the point of view of sediment dynamics) is the presence of a vast asymmetric moraine ridge in the nearshore of the KI. This massive underwater landform is located in approximately 4—7 m deep water and is intensely affected by submarine erosion. This ridge covers an elongated in the NWW direction area that is about 10 km long and up to 4 km wide. Coarse-grained boulder-pebble sediments with clayey diamicton outcrops interspersed with patches of sand dominate in this area

In the nearshore between the shoreline and 1—1.5 m isobaths a stable system of longshore and fan-shaped sand ridges partly adjoined to the coastal line is observed. The best-balanced sand ridges (with the total width of the sand ridge zone up to 600 m) are in the north-eastern part of the submarine coastal slope of the study area. The bottom of the area of sand ridges is smooth and the maximal relative height of the ridges is about 0.5 m. The ridges are composed of coarse- to medium-grained (Ma varies from 0.4 to 0.9 mm, an average is 0.7 mm) and usually poorly sorted sand (So 1.8—2.4). Well sorted (So 1.0—1.5) fine-grained sands (Ma 0.2 mm) form longshore ridges only in the eastern part of this coastal slope.

According to drilling results (e.g. sites KDT-15, Fig. 4A), the upper sediment layer (0—5 cm) of the runnels between the sand ridges is composed of poorly sorted (So > 2.0) medium- to coarse-grained sands with high (up to 25—30 %) content of gravel material. This layer is underlain (depth 5—25 cm) by fine-grained sands with low content of silty-clayey particles. This low content indicates the periodic reworking of this layer by waves. The location of fine-grained clayey sands (at depths 25—30 cm) and pure clays or clayey diamicton (at depths below 30 cm) apparently indicate the lower boundary of wave impact in the sediment layer. Consequently, the thickness of the active sediment layer is about 30 cm (fig. 4, *a*).

The gently sloping onshore coastal landscape peaks with smooth up to two metres high sand dunes in the backshore that separate the low coastal terrace from the sea. The old embankment located along the southern coast of the KI is, in essence, a technogenic barrier. A series of cross-bedded sand layers indicates the direction and rate of beach accretion and erosion (fig. 5, see an insert). The upper part of the sediment sequence is composed of fine-grained (Ma 0.1—0.22 mm) well-sorted (So 1.0—1.2) sands. The GPR profiles allowed tracing the lower boundary of the sand layer. This boundary is a clayey surface below which the GPR signal is lost. The thickness of the sand layer within the beaches of western KI varies from 20—30 cm in the nearshore to 2—2.5 m in the dunes. These results are a crucial input for the modelling of storm impact on beach profiles.

3.2. Geological processes driven by external forcing. The shoreline of the western KI has a cuspate shape formed by smooth glacial moraine capes and pocket beaches between them. The coasts here are heavily eroded (fig. 1). The local sand accretion areas are in certain smooth bays of the eastern part of the study area. The maximal rate of recession of the coastline (2 m/year) is observed in the westernmost section of the KI near the fort «Reef». The rate of coastal erosion in the adjacent coastal segments is 0.5—1 m/year with minimal erosion rates around themoraine capes. Sand accretion with rates of 0.3—0.4 m/year takes place in the easternmost part of the study area.

A comparison of recent coastal observations with the outcome of similar observations made in 2008 confirmed the results extracted from the remote sensing data. The shoreline contains of interspersed active erosion escarpments and broken fortification and coast protection structures that keep some sections of the shoreline more stable. In places wavelike features (local disturbances to the otherwise mostly straight beach plane) are evident. They are characterized by a wide accretion downdrift end and a narrow, erosion updrift end. Such longshore sand waves are formed within the intense longshore sand drift to the east. The material for these structures comes from actively eroded western coasts of the study area.

Therefore, intense erosion predominates in the geological and geomorphic features of the coastal zone of the western KI. The main consequences of extremely active erosion processes are: 1) wide spreading of boulder-pebble benches in the nearshore seabed, indicating significant sediment deficit; 2) very small (less than 30 cm) thickness of the active sand layer in the longshore sand ridge system, 3) prevailing of narrow (10—15 m) sand beaches and 4) low and smooth offshore and onshore landscape (the foredune height is less than 2 m).

Based on the revealed features it is possible to recommend artificial sand nourishment as the main method to mitigate sediment deficit and to prevent the future erosion. The necessary amounts of sand refill as well as other parameters of the artificial beach are discussed in section 5.4.

4. Numerical experiments. The construction and operation of the FPB have led to a strong change in the hydrologic conditions in the vicinity of the KI. We consider the time interval from the beginning of the functioning of the FPB in August 2011 till the present. The analysis of sea level time series recorded in the stations «Ozerki» and «Kronstadt» (fig. 2, *b*) has shown that during this time interval the maximum water levels were observed in 2011. Three storm surges in the Neva Bay in November–December 2011 required the FPB gates to be closed to prevent flooding in Saint Petersburg. A flooding in this city occurs when the water level rises higher than 160 cm above the long term mean of the Kronstadt sea level gauge (denoted as the Kronstadt zero). The first one occurred on November 27—28. The two other surges occurred one after another on December 26—28 during the passage of a deep cyclone. During the time interval in question three water level peaks were recorded in the hydrological station «Gornyi Institute» (59°55′44″ N, 30°16′12 E): 142, 156 and 170 cm above the Kronstadt zero.

We simulate the strongest flood event that occurred on December 26—28, 2011. The initial conditions for the circulation model such as water temperature and salinity were taken from the HIROMB model [28]. The initial current velocities were assumed to be zero. At the open western boundaries (fig. 2, *b*) we used the hourly sea level time series recorded in the «Shepelevo» hydrological station (fig. 2, *b*). The temperature and salinity of water at the boundary was set constant and equal to the initial values of these parameters. At the eastern boundary the water temperature was set to a constant value of +2 °C and water salinity to zero to match the water from the River Neva. The discharge of this river was assumed to be equal to its average climatic value for December (2030 m^3/s) and was distributed among the river branches. The spin-up time of the circulation model was 3 hours.

At the sea-atmosphere interface we used the hourly values of the main meteorological parameters (atmospheric pressure, air temperature, relative humidity, wind speed and direction, cloudiness, precipitation rate) calculated by the HIRLAM model (High Resolution Limited Area Model) (http://hirlam.org). We employed the results of model runs performed at the SMHI (Swedish Meteorological and Hydrological Institute). The SMHI runs an operational short-range numerical weather prediction system that uses the HIRLAM model on a domain covering Europe and the adjacent North Atlantic with a horizontal resolution of approximately 11 km and 40 vertical hybrid levels. Lateral boundaries for these runs come from the European Centre for Medium-Range Weather Forecasts (ECMWF) BC project with a 3-hour time resolution [29].

The accuracy of replication of the storm surge is largely determined by the adequacy of the wind information. A comparison of the wind characteristics calculated by the HIRLAM model with the observations at the station «Ozerki» (the outer side of the FPB) showed very good agreement for the time interval of December 26—28, 2011.The average values of wind speed U_{mod} from the HIRLAM model and from the measurements had a correlation coefficient of $R = 0.84$. The values estimated by the HIRLAM model exceeded the observed ones on average by 1.2 m/s (12 %) and the wind directions φ differed on average by 4° ($R = 0.96$). For measurement sites in Kronstadt and Lomonosov (60.55° N, 28.20° E) located on the inner side of the FPB on the coast of the Neva Bay the agreement was somewhat worse. The correlation coefficient for U_{mod} was $R = 0.82$ in both cases. Similarly to the above, the modelled values of Umod exceeded the observed values by 3.7 and 3.2 m/s,

respectively.The correlation coefficients for the angle φ were $R = 0.78$ and $R = 0.90$, respectively, with average differences in the directions 7.5° and 4°, respectively, in Kronstadt and Lomonosov. Therefore, the HIRLAM model slightly (but not too much) overestimates the wind speed during the three extreme hydrometeorological situations and almost accurately reproduces its direction.

Two typical beach profiles from the erosion areas on the southern and northern coasts of the KI (called Kotlin–south and Kotlin–north, respectively, fig. 6) were chosen as a geomorphic base for the modelling efforts. In both areas a very gentle bottom slope in the nearshore and in the vicinity of the waterline turns into a relatively steep beach scarp or a foredune with a height of about 2.5 m. The characteristic size of the sand particles is 0.25 mm.

5. Results

5.1. Sea level and currents. As discussed above, the most severe floods from the commencement of the operation of the FPB occurred on December 26—28, 2011. To reproduce these events a reference model run was performed with the external forcing described in Section 4, including the wind input from the HIRLAM model. The verification of the model was carried out against sea level data from the hydrological station «Gornyi Institute». The model underestimates the peaks in sea level by 45 cm but adequately represents the timing of the observed water level maxima on December 26, 2011 and December 28, 2011 (fig. 7).

There are at least three reasons for this discrepancy: 1) the limitations of the hydrodynamic model, 2) the assumption that the sea level is constant at the open sea western boundary, 3) the ignoring of the wind gustiness. Previous studies [9, 15] indicated that the model itself is sufficiently adequate for the study area. Unfortunately, there are no reliable data on the sea level changes across the Neva Bay. To mimic the wind

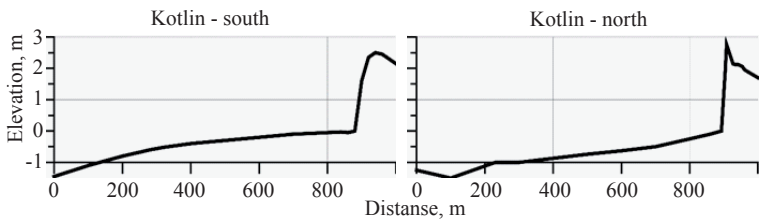

Fig. 6. The typical beach profiles on the southern and northern coasts of the KI.

Рис. 6. Типичные профили пляжа на южном и северном побережьях о. Котлин.

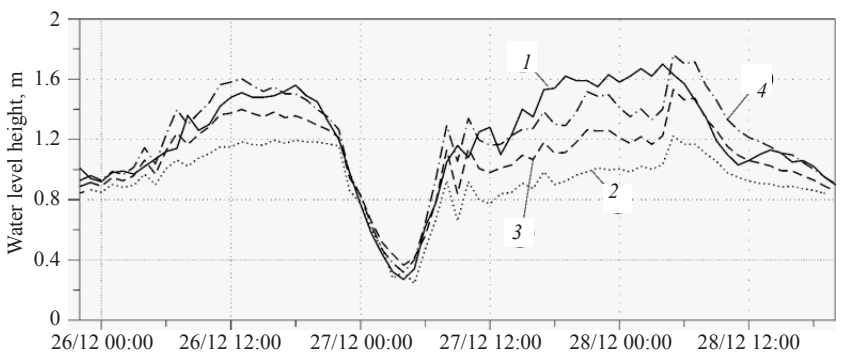

Fig. 7. The course of water level in the "Gornyi Institute" station on December 26—28, 2011, based on observations (*1*) and on model results forced using the HIRLAM model data adjusted with the values of the wind coefficient k=1 (*2*), k=1.37 (*3*) and k = 1.61 (*4*). The mean value and mean-square deviation of sea level from observations and from the outcome of the calculations with k = 1, 1.37 and 1.61 are 1.20 and 0.93, 1.08 and 1.22, 0.34 and 0.21, 0.25 and 0.32, respectively.

Рис. 7. Ход уровня воды на станции «Горный институт» 26—28 декабря 2011 г., основанный на данных наблюдений (*1*) и на результатах расчета при задании скорости ветра из модели HIRLAM, скорректированной со значениями коэффициента k = 1 (*2*), k = 1.37 (*3*) и k = 1.61 (*4*). Среднее значение и среднеквадратичное отклонение уровня моря для данных наблюдений и результатов расчетов с k = 1, 1.37 и 1.61 составляют 1.20 и 0.93, 1.08 и 1.22, 0.34 и 0.21, 0.25 и 0.32, соответственно.

gustiness and possibly elevated water levels to the west of the study area we introduced a certain adjustment (an extra coefficient) of the wind speed. The justification for such an adjustment is that the contribution of wind gusts to the wind effect on the sea surface can be significant.The ratio of the maximum wind gust of standard observations to the average wind speed (over a 10-minute time interval) in the station «Ozerki» was 1.4—2.2 on December 26—28, 2011 with an average value of 1.65. The impact of wind gusts is often taken into account by means of introducing a sort of random fluctuations to the wind forcing. In this paper we prefer to remain within the deterministic approach. In order to take into account wind gusts we performed two additional model runs in which the wind speed reproduced by the HIRLAM model was multiplied by a certain coefficient k (called wind coefficient in fig. 7) during the entire simulation. We used the values k = 1.37 (run 1) and k = 1.61 (run 2). A fairly good agreement between the calculated and measured sea levels in the «Gornyi Institute» station was achieved in the run 2 (fig. 7), i.e. when the modelled wind speed was increased by 61 %.

We start the discussion of properties of modelled sediment transport near the southern and northern coasts of the KI from the results of the reference run that was forced with unadjusted outcome of wind information from the HIRLAM model. The results of runs with the adjusted wind will be discussed below in Section 5.4.

Fig. 8 shows an example of the pattern and distribution of surface velocities during a storm on December 26, 2011. The currents near both coasts (northern and southern) of the western part of the KI were mostly oriented from the northwest to the southeast. Only during the initial phase of the storm surge (from 0:00 to 5:00 on December 26, 2011) the currents along the southern coast were either unstable or directed to the northwest. During the water level peak in Shepelevo on December 26, 2011 (fig. 8) and on December 27, 2011 the speed of currents was 20—60 cm/s near the southern coast and 20—80 cm/s near the northern coast. The current speed reached more than 100 cm/s at the westernmost point of the KI. The current speeds were much smaller and did not exceed 30—40 cm/s (except for the westernmost nearshore of the KI) when the water was relatively low on December 27, 2011 (between two surges) and during the relaxation phase of the surge in the evening of December 28.

5.2. Wind waves. The spatial distributions of significant wave heights (SWH) were also simulated using the wind speed from the HIRLAM model. Fig. 9 (see an insert) presents the SWH at the time of the observed sea level peak in Shepelevo on December 26. Importantly, the SWH near the coast during the two storm surges was approximately 1.5 times as high as the SWH in the evening of December 28 (fig. 10, see an insert) when the water level was no more significantly elevated.

5.3. Shore dynamics. The longshore sediment transport in the coastal zone is driven by the joint action of waves and currents. A commonly accepted view is that sediments are mobilised primarily due to orbital wave velocities and then transported by the longshore current. On very shallow and gentle coastal slopes that are typical in the study area (fig. 6) the current induced by breaking waves is comparatively weak (usually ≤0.3 m/s) and the dominant role in the relocation of sediment parcels play nearshore currents driven by the storm. Calculation of the transport of sediment during the storms on December 26—28, 2011 is based on computations of properties of storm surge, wind waves and currents for selected coastal profiles (fig. 6). The input parameters are selected for nearshore sea points with a water depth of 7.3 m and 8.1 m, respectively,

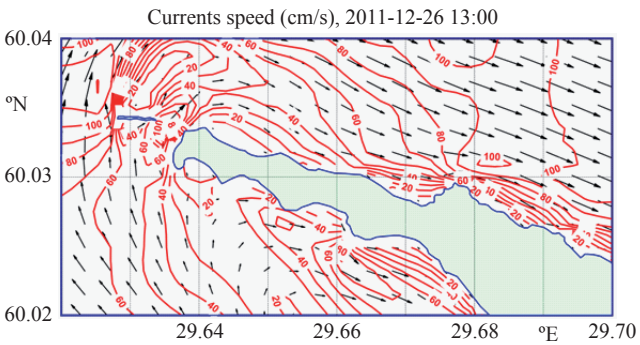

Fig. 8. Modelled surface currents near the western part of the KI for the model run with unadjusted wind information from the HIRLAM model (k = 1).

Рис. 8. Рассчитанные поверхностные течения вблизи западной части о.Котлин для расчета с нескорректированной информацией о ветре из модели HIRLAM (k = 1).

near the southern and northern coasts of the KI. Notice that both these points are located outside the original profiles. The major features of temporal changes in the SWH and the height of storm surge during the storm are very similar for both sites (Kotlin–south and Kotlin–north, fig. 11).

However, the properties of storm-generated currents show noticeable differences near the southern and northern coasts. To the south of the KI the current speeds do not exceed 0.3 m/s, but their directions vary significantly. To the north of the KI the currents are predominantly unidirectional (to the east) while their speeds reach 0.7 m/s. The temporal variations in the total net longshore sediment transport q_{total} and the bulk sediment transport Q during the storm are shown in fig. 12. As a certain amount of sediment is transported alongshore also in areas that are deeper than the limiting depths of the above profiles, the values q_{total} and Q should be treated as the minimum estimates of the net and bulk shore-parallel sediment transport.

Fig. 11 and 12 indicate that the temporal course of net alongshore transport basically matches the similar course of the SWH and the storm surge height. The maximal net transport reaches 0.8×10^3 m^3/h and 1.7×10^3 m^3/h on the southern and the northern coast of the KI, respectively. Between the storms the longshore transport almost ceases. The simulated bulk sediment transport along the southern coast of the KI is 18×10^3 m^3. The transport along the northern coast is 52×10^3 m^3, that is, three times as high as on the southern coast (fig. 12). This difference is due to a much higher intensity of storm currents along the northern coast of the KI.

The calculated storm-induced changes in the two coastal profiles during two storms on December 26—28, 2011 are presented in fig. 13. For a better comparison we present the profiles at the beginning and the end of the storms together with an intermediate profile formed during the first storm (24 hours after the start). Since the changes are concentrated on the beach and the foredune, only the upper part of the coastal slope is shown.

Fig. 13 depicts the classic cutting process of the beach and foredunes. During elevated water levels the waves reach the top of the foredune and erode it. The eroded material is deposited seawards from the dune foot across the entire equilibrium beach profile. As a result, the surface of the dune is lowered, the beach expands towards the sea and the beach profile becomes flatter. Fig. 13 demonstrates that the northern coast is more vulnerable with respect to the joint impact of elevated water levels and high waves. The height of the dune crest here decreases by 0.6 m by the end of the second storm.

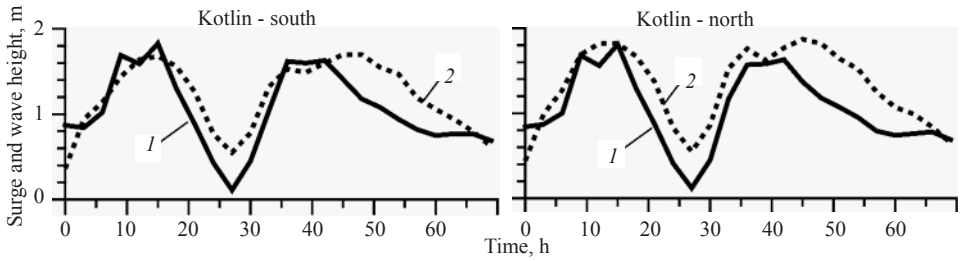

Fig. 11. The temporal course of the storm surge height (*1*) and SWH (*2*) during the two storms on December 26—28, 2011 in selected sites.

Рис.11. Временной ход высоты штормового нагона (*1*) и ЗВВ (*2*) во время двух штормов 26—28 декабря 2011 г. в выбранных местах.

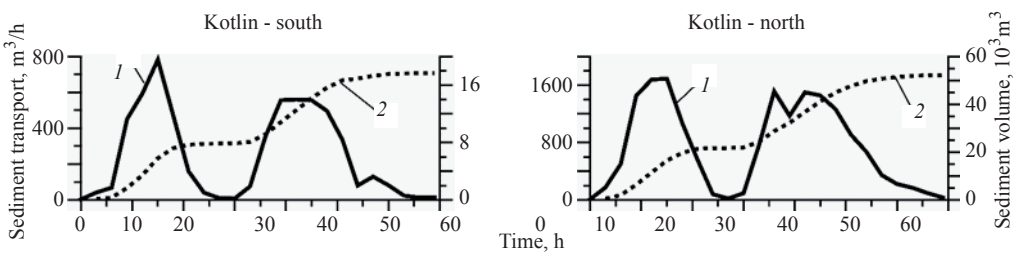

Fig. 12. Simulated time series of the total net longshore sediment transport q_{total} (*1*) and the bulk sediment transport Q (*2*) on December 26—28, 2011.

Рис.12. Рассчитанные временные ряды общего вдольберегового переноса осадков q_{total} (*1*) и объема переноса Q (*2*) 26—28 декабря 2011 г.

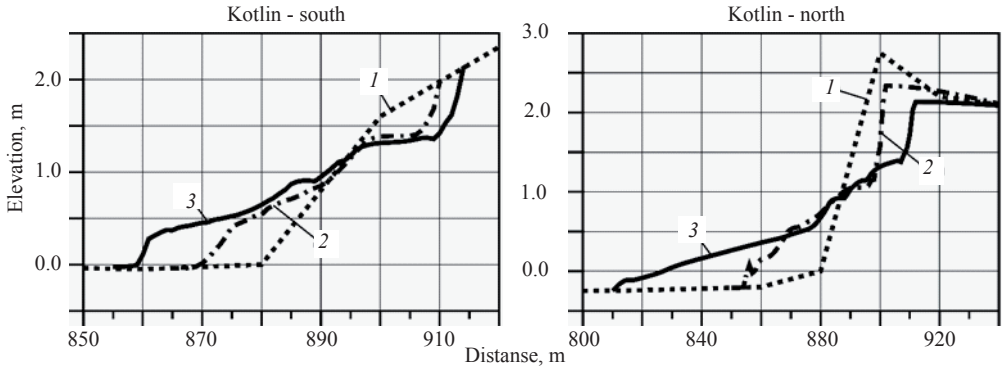

Fig. 13. Simulated storm-induced deformations of coastal profiles:
1 — initial state, *2* — 24 hours after the storm start, *3* — final state.

Рис. 13. Рассчитанные деформации прибрежных профилей, вызванные штормом:
1 — начальное состояние, *2* — через 24 ч после начала шторма, *3* — конечное состояние.

It should be noted that the removal of the material from the upper part of the foredune is apparently irreversible in the study area. Differently from the classic "cut and fill" process on the open ocean coasts where sediments predominantly move across the shore, sediments cannot return in the equal volume here since an appreciable part of them is transported along the shore to a different location. Moreover, in the Baltic Sea the proportion of regular long-period swells is very low. The majority of moderate and weak wave conditions represent relatively steep waves and situations with the height of storm surge $\eta<0.5$ m and SWH<0.5 m [21] that do not restore sand volumes on the beach. Such a behaviour deviates essentially from the classical scheme in which the low waves tend to restore the beach eroded by a storm. The difference is due to the effect of both the extremely high storm surges and the predominance of relatively short steep waves in the study area.

5.4. Shore-protecting artificial beach. According to the recommendations of geologists (part 3.1) the best way to protect the coasts in the study area is to create artificial beaches. Their characteristics may be determined by the parameters of an extreme representative storm event (the calculation procedure is described in Appendix 1). We assume that such a case could be the storm on December 26—28, 2011 which was the maximum one from August 2011 to the present time. We performed calculations for three different wind coefficients (see Section 5.1) that corresp to $k = 1$, $k = 1.37$, and $k = 1.61$. The initial information on the SWH H_s and wave period $\overline{T}$, as well as the height of the storm surge η, are shown in table. The maximum sea level elevation is limited to 2 m.

According to a well-known general recommendation, the materials coarser than the natural ones are better suited to create an artificial beach [2]. The representative particle size of natural sand in the study area is d_g=0.25 mm. Two options for the artificial beach were considered: medium sand (d_g=0.5 mm) and very coarse sand (or granule, d_g=2.0 mm). The simulated parameters of the artificial beach are shown in table and the associated beach profiles at $k = 1$ in fig. 14.

One prescribed parameter, the advance of the shore X, in most cases was taken to be 20 m. This width is usually large enough to provide a necessary reserve of the beach material. Only if medium (0.5 mm) sand would be used in the Kotlin–north section, this advance X should be at least 40 m (table; fig. 14). The main calculated characteristics of the artificial beach are its maximum elevation above the still-water level z_m and the width of the berm l_a (fig. 14). These parameters define the volume of the building material V per unit length of the beach (table).

With increasing the particle size d_g, the elevation z_m, l_a and V increase usually as well. This is due to the increase in both the profile slope and the height of the wave run-up (see Appendix 1). However, due to a lesser loss of the coarse material, the volume V could be reduced by decreasing the shore advance X (see the cases of Kotlin–north at $k = 1$ and $k = 1.61$). With increasing wind, for the southern coast the required volume of building material V increases by 1.2 times for medium sand and 1.4 for granules; the effect of increasing the particle size with the same wind turned out to be much stronger: the volume increases by 3.7, 3.2 and 3.1 times for $k = 1$, $k = 1.37$ and $k = 1.61$, respectively. For the northern coast, the volume V depends insignificantly on both the wind forcing and the increase in particle size.

Initial data and calculated parameters of the artificial beach profiles for different values of the wind coefficient *k*

Исходные данные и расчетные параметры искусственных профилей пляжа для разных значений ветрового коэффициента *k*

k = 1 Section of the coast	H_s, m	$\overline{T}$, s	η, m	*X*, m	d_g, mm	z_m, m	l_a, m	*V*, m³/m
Kotlin–south	1.7	4.5	2.0	20	0.5	2.53	29.5	22.3
					2.0	2.74	56.9	83.1
Kotlin–north	1.9	4.8	2.0	40	0.5	2.61	5.6	55.6
				20	2.0	2.86	13.2	53.4
k = 1.37 Section of the coast								
Kotlin–south	2.4	5.2	2.0	20	0.5	2.69	24.5	30.8
					2.0	2.98	50.7	97.0
Kotlin–north	2.8	5.7	2.0	40	0.5	2.79	1.0	55.4
				20	2.0	3.12	7.7	55.8
k = 1.61 Section of the coast								
Kotlin–south	2.7	5.4	2.0	20	0.5	2.74	22.9	32.0
					2.0	3.04	49.2	99.3
Kotlin–north	3.2	6.0	2.0	40	0.5	2.86	0.0	57.5
				20	2.0	3.21	5.4	55.1

The loss of sediments due to the longshore transport increases with the increase in annual bulk sediment transport Q_{max} (see Appendix 1). Using the estimates of the bulk transport obtained for the extreme storm on December 26—28, 2011 as reference values (fig. 12), the bulk transport Q_{max} would be approximately 2×10^4 and 5×10^4 m³/year for the southern and northern sections, respectively. These values refer to the natural sand with the mean grain size d_g=0.25 mm. For building sands with d_g=0.5 and 2.0 mm, the corresponding values of Q_{max} will decrease to 1×10^4 and 0.4×10^4 m³/year for the southern section and to 3×10^4 and 1.4×10^4 m³/year for the northern section, respectively. The calculations of sediment losses based on formula (A5) in Appendix 1 and the use of the above-mentioned estimates indicate that for a beach that consists of coarse sand or gravel and with a length of at least 1000 m, more than half of its volume can be preserved after 20 years.

6. Discussion. When examining table, the following question arises. Why are there such significant differences in the volume of building material for the southern and northern coasts? As can be seen in fig. 14,

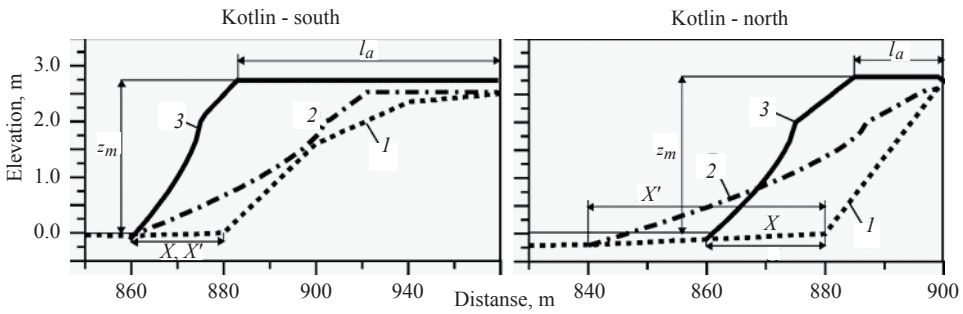

Fig. 14. Calculated profiles of the artificial beach at *k* = 1: *1* — natural profile, *2* and *3* — artificial profile in case of sand of 0.5 mm and gravel of 2.0 mm, respectively. *X'* is the advance of the shore in the case of sand of 0.5 mm.

Рис. 14. Расчетные профили искусственного пляжа при *k* = 1: *1* — естественный профиль, *2* и *3* — искусственный профиль в случае песка 0.5 мм и гравия 2.0 мм, соответственно. *X'* — продвижение берега в случае песка 0.5 мм.

the matter is in the nature of the initial beach profiles. On the southern coast it is gentler, and for the construction of a steep profile a lot of material is required. On the northern coast, the original profile is initially steep and less material is needed to create a necessary profile.

Another important question: why are there practically no wind effects for the northern coast? With the increase in wind speed, the height of the profile should be greater, and therefore, more building material should be foreseen. However, the lower part of the profile becomes shallower, the upper part of the profile is shifted towards the shore, and the width of the berm is reduced. These features together mean that less building material is necessary. Both effects compensate each other, and the volume of the building material remains almost unchanged.

Extreme events like the storm on December 26—28, 2011 do not happen every year and the average background rates of the longshore sediment transport in the study area are likely below the estimated values of Q_{max}. The results of coastal monitoring carried out by the VSEGEI since 2000 indicate that the frequency of extreme coastal erosion events such as driven by the storms on December 26—28, 2011 has drastically increased during the last years. According to the North-West Department of Hydrometeorological Service, 13 floods occurred in Saint Petersburg in 2011—2016. The percentage of days in the year with the sea level exceeding 1 m near the FPB was 35 % in 2011, 5 % in 2013, and 70 % in 2015. Such water levels were not observed in 2012, 2014 and 2016. Thus, the most active destruction of the Kotlin coasts over the 6-year period occurred during 18 % of the time. However, it should be taken into account that under conditions of insignificant surge and moderate waves the beach is eroded too (due to short steep waves that are typical in the study area) and the longshore sediment transport continues as well. Therefore, the actual typical values of the bulk annual longshore sediment transport apparently are comparable with the estimated above values of Q_{max}.

When building an artificial beach from a coarser material a larger amount of this material is required to provide a required advance of the coast. An increase in the beach length leads to an increase in the costs at the initial stage of construction. However, the relative losses of material due to storm impacts and longshore sediment transport are reduced. This in turn decreases the cost of the beach maintenance. Therefore, the choice of optimal characteristics of an artificial beach should express a trade-off between different interests.

Summary

1. The coastline retreat rates in the western part of the Kotlin Island identified by retrospective analysis reach 1.2—1.6 m/year and are among the highest in the eastern part of the GoF, which should be taken into account in forecasting the development of the coast and paleogeographic reconstructions.

2. Extensive geological nearshore and onshore studies revealed the following geological and geomorphic features of the western KI coastal zone: 1) wide spreading of boulder-pebble benches in the nearshore indicating significant sediment deficit, 2) very small (not more than 30 cm) thickness of the active sand layer within longshore sand ridge system, 3) predominance of narrow (10—15 m) sand beaches, and 4) low and smooth offshore bathymetry and onshore landscape.

3. A coupled mathematical model including models of circulation, wind waves, and sediment dynamics was developed. Calculations of current velocities were performed using the 3D hydrodynamic model of the eastern part of the GoF and the Neva Bay [9]. The calculation of waves was carried out using the SWAN wave model. Changes to the coastal profiles due to storms were calculated using the CROSS-P model [4]. Initial data for these calculations were the initial depth, sediment characteristics (average size, density, porosity), wave parameters (height, period, angle of wave approach relative to the cross-shore direction), height of the storm surge, wind speed, and duration of a storm.

4. The coupled model was used to determine the parameters of artificial sand nourishment as a major method to compensate sediment deficit and to prevent the future erosion. Given the actual external forcing (atmospheric forcing from the HIRLAM model, open boundary conditions from the HIROMB model, bathymetry and beach topography from the geological data sets), the parameters of artificial beach profiles have been calculated to meet the maximum storm surge and the annual volume of sand necessary for the conservation of the artificial beach has been estimated.

5. The proposed method aimed to sustainable maintenance of sand beaches can be applied to other coastal areas of the Baltic Sea, as well as to other seas.

Appendix 1. A MODEL OF AN ARTIFICIAL BEACH

Profile geometry. A scheme of profiles of natural and designed beaches is given in fig. A1. The elevation z is measured from the still water level and the horizontal distance x is counted seawards from the highest beach point (defined as the sum of the storm surge η and wave run-up R heights).

A horizontal segment l_a corresponds to the berm width. Its variations allow displacement of the whole designed profile seaward or landward in order to achieve its intersection with the natural profile at the closure depth h_*. The latter limits the area of significant bed deformations.

The distance l_R is a length of wave run-up. It depends on the run-up height R and the equilibrium slope β_R:

$$l_R = R/\beta_R,\ R = \beta_R\sqrt{H_s L},\ \beta_R = 0.12\left(\frac{T_p\sqrt{gd_g}}{H_{sB}}\right)^{0.5}, \tag{A1}$$

where H_s and $L = (g/2\pi)T_p^2$ are the deep-water significant wave height and length, T_p is the period of spectral peak, H_{sB} is the breaking wave height, d_g is the representative sediment grain size. The values of R and β_R are computed from the relationships presented in [30, 31].

A segment l_* corresponding to the underwater part of the designed profile under storm surge conditions is defined using Dean's equilibrium profile [2]:

$$h = Ax^{2/3},\ A = 2.25\left(w_g^2/g\right)^{1/3}, \tag{A2}$$

where h is water depth relative to the storm surge level, w_g is the grain settling velocity in water, and g is acceleration due to gravity. The parameter A is of the order of 10^{-1} $m^{1/3}$ and increases as the grain size grows. The length of the segment is $l_* = (h_*/A)^{3/2}$. The closure depth h_* is assumed equivalent to the wave breaking depth h_B:

$$h_* = h_B,\ h_B = \left(\frac{1}{4\pi\gamma_B^2}\right)^{2/5} H_{1\%}^{4/5}\left(gT_p^2\right)^{1/5}, \tag{A3}$$

where $\gamma_B = 0.8$ is the breaker index, $H_{1\%}$ is the height of 1 % cumulative exceedance in the wave ensemble [4, 20].

The difference between coastline positions of the designed and natural profiles, $X = x_0 - x_0'$, defines the advance of the shore within the artificial beach.

The volume of the material V per unit length of the coastline (m^3 m^{-1}) required for the beach construction can be found as

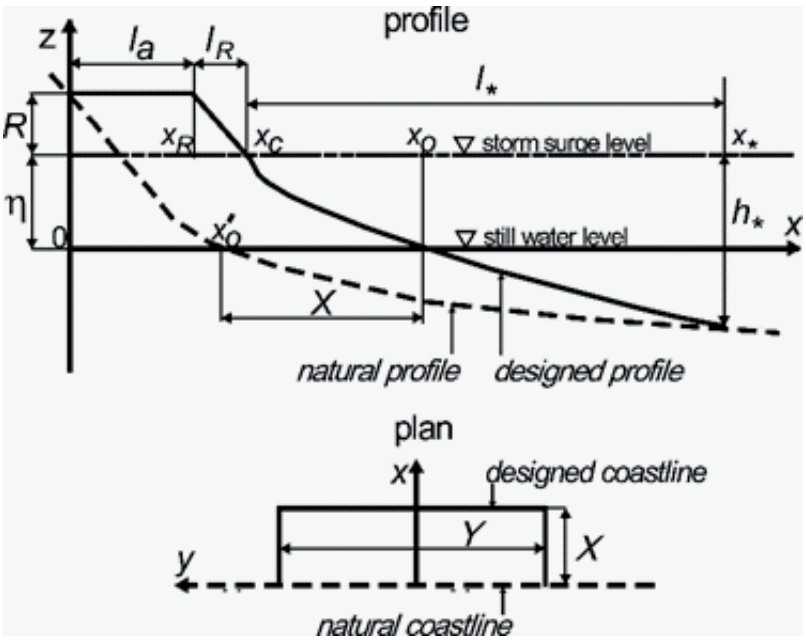

Fig. A1. A scheme of an artificial beach. The notations are given in the text.

Рис. А1. Схема искусственного пляжа. Обозначения указаны в тексте.

$$V = \int_0^{x_*} (z - z')dx, \tag{A4}$$

where z and z' are the elevations of artificial and natural profiles relative to the still level.

On very gentle coastal slopes (typical in the eastern Gulf of Finland), the closure depth h_* may occur at a long distance from the coast. This means that the designed beach would be too wide and unacceptable from the practical viewpoint. In this case the advance of the coast X should be limited. A decrease in X leads to some decrease in the closure depth h_*. If this reduction is not very large, it does not disturb the stability of the beach profile.

Beach material loss. The planform of the artificial beach looks like a distribution of the shoreline in a rectangular form of the cross-shore width X and along-shore length Y (fig. A1). Affected by the longshore sediment transport the beach volume will decrease with time and the beach planform will change (fig. A2).

The process is described by the mass conservation law which, under certain conditions, takes a form of a diffusion equation [2]. According to Dean's results the material volume $V(t)$ within the beach boundaries in relation to initial volume V_0 can be approximately estimated as

$$\frac{V(t)}{V_0} = 1 - \frac{2}{\sqrt{\pi}} \frac{\sqrt{Gt}}{Y}, \; G = \frac{\hat{Q}}{(h_* + R)}, \tag{A5}$$

where G is a diffusion coefficient (m^2/year) and $\hat{Q}$ expresses the double maximal capacity of the bulk longshore sediment transport $Q_{\max}$ (m^3/year). The loss of material decreases with an increase in the beach length Y and a decrease in the bulk sediment transport $Q_{\max}$. The latter can be reduced by using coarser sediments.

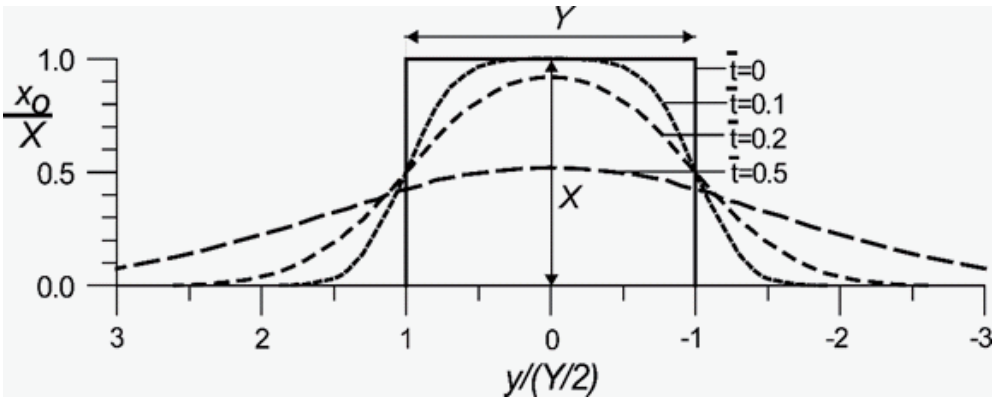

Fig. A2. Evolution of the artificial beach shoreline. The non-dimensional time is $\bar{t} = \sqrt{Gt}/Y$.

Рис. А2. Эволюция береговой линии искусственного пляжа. Безразмерное время равно $\bar{t} = \sqrt{Gt}/Y$.

This research was a part of the project «Development of General Scheme of Coast Protection of the marine coasts of Saint-Petersburg City» funded by the Committee for Natural Use, Environmental Protection and Ecological Safety of Saint-Petersburg. The results of sections 2.2, 5.1 and 5.2 where obtained in the framework of the state assignment of FASO Russia (theme No. 0149-2018-0014). V. A. Ryabchenko and S. D. Martyanov were supported by the grant 14-50-00095 of the Russian Science Foundation. A. Yu. Dvornikov, V. A. Ryabchenko and S. D. Martyanov were supported by the grant 16-55-76021 of the Russian Foundation for Basic Research (RFBR). I. O. Leont'yev was supported by the grant 15-05-08239 of RFBR. A. Yu. Sergeev and D. V. Ryabchuk were supported by the Russian Science Foundation for retrospective analysis of coastal deformations (grant 17-77-20041). The authors are sincerely grateful to the reviewers for valuable comments that have made it possible to improve the paper.

Литература

1. *Hanson H.* GENESIS: a generalized shoreline change numerical model // J. of Coastal Res. 1989. V. 5, N 1. P. 1—27.
2. *Dean R. G.* Beach Nourishment: Theory and Practice. World Scientific Inc., 2002. 399 p.
3. *Van Rijn L. C.* et al. Numerical modeling of erosion and accretion of plane sloping beaches at different scales // Coastal Engineering. 2011. V. 58. P. 637—655.

4. *Leont'yev I. O.* Morphodynamic Processes in the Coastal Zone of the Sea. Saarbrücken: LAP LAMBERT Academic Publishing, 2014. 251 p.
5. *Ryabchuk D.* et al. Long term and short term coastal line changes of the Eastern Gulf of Finland. Problems of coastal erosion // Journal of Coastal Conservation. 2012. V. 16, N 3, P. 233—242.
6. *Van Rijn L. C.* et al. The predictability of cross-shore bed evolution of sandy beaches at the time scale of storms and season using process-based profile models // Coastal Engineering. 2003. V. 47. P. 295—327.
7. *Roelvink D.* et al. Modelling storm impacts on beaches, dunes and barrier islands // Coastal Engineering. 2009. V. 56. P. 1133—1152.
8. *Романовский С. И.* Физическая седиментология. Ленинград: «Недра», 1988. 239 с.
9. *Ryabchenko V.* et al. Modelling ice conditions in the easternmost Gulf of Finland in the Baltic Sea // Continental Shelf Research. 2010. V. 30. P. 1458—1471. Doi: 10.1016/j.csr.2010.05.006
10. *Рябченко В. А., Коноплев В. Н., Кондратьев С. А., Поздняков Ш. Р., Лыскова У. С.* Оценка изменения качества воды Невской губы после введения в эксплуатацию Юго-западных очистных сооружений Санкт-Петербурга (по данным математического моделирования) // Изв. Русского Географического Общества. 2006. Т. 138, Вып. 5. С. 48—57.
11. *Андреев П. Н., Дворников А. Ю., Рябченко В. А., Цепелев В. Ю., Смирнов К. Г.* Воспроизведение штормовых нагонов в Невской губе на основе трехмерной модели циркуляции в условиях маневрирования затворами Комплекса Защитных Сооружений // Фундаментальная и прикладная гидрофизика. 2013. Т. 6, № 4. С. 23—31.
12. *Blumberg A. F., Mellor G. L.* A description of a three-dimensional coastal ocean circulation model. / Heaps N. (Ed.), Three-dimensional Coastal Ocean Models. American Geophysical Union, 1987. P. 208.
13. *Booij N.* et al. A third-generation wave model for coastal regions, Part 1. Model description and validation // Journal of Geophysical Research. 1999. V. 104 (C4). P. 7649—7666.
14. *Ris R. C.* et al. A third-generation wave model for coastal regions, Part 2. Verification // Journal of Geophysical Research. 1999. V. 104 (C4). P. 7667—7681.
15. *Martyanov S., Ryabchenko V.* Bottom sediment resuspension in the easternmost Gulf of Finland in the Baltic Sea: A case study based on three–dimensional modeling // Cont. Shelf Res. 2016. V. 117. P. 126—137. Doi: http://dx.doi.org/10.1016/j.csr.2016.02.011
16. *Bagnold R. A.* Mechanics of marine sedimentation // The Sea. V. 3. N.Y.: J. Wiley, 1963. P. 507—528.
17. *Bowen A. J.* Simple models of nearshore sedimentation; beach profiles and longshore bars // Coastline of Canada. Geol. Surv. Can. Halifax, 1980. P. 1—11.
18. *Leont'yev I. O.* Coastal Dynamics: Waves, Currents, Sediment Transport. M.: GEOS, 2001. 272 p.
19. *Leont'yev I. O.* Modeling the morphological response in a coastal zone for different temporal scales // Advances in Coastal Modeling / Ed V. C. Lakhan. Amsterdam, The Netherlands: Elsevier Science Publishers, 2003. P. 299—335.
20. *Leont'yev I. O.* Calculation of Longshore Sediment Transport // Oceanology. 2014a. V. 54, N 2. P. 226—232.
21. *Leont'yev I. O.* et al. Modeling of Storm-Induced Deformations of a Sandy Coast (Based on the Example of the Eastern Gulf of Finland) // Oceanology. 2015. V. 55, N 1. P. 131—141.
22. *Leont'yev I. O.* et al. The Forecast of Coastal Recession in the Eastern Gulf of Finland for the Twenty-First Century // Oceanology. 2015a. V. 55, N 3. P. 434—440.
23. *Leont'yev Igor, Akivis Tatiana.* An artificial beach as a means for sea coast protection from storm surges (by the example of the Eastern Gulf of Finland) // Proc. of Int. Conf. "Managing risks to coastal regions and communities in changing world" (EMECS'11 – Sea Coasts XXVI). 2017.
24. URL:https://www.google.com/url?q=https%3A%2F%2Fdoi.org%2F10.21610%2Fconferencearticle_58b4315f8fc73&sa=D&sntz=1&usg=AFQjCNGPEkTFBEreOx2JE-ApS5YELG6ahg (Дата обращения: 20.04.18).
26. Geological Atlas of St. Petersburg. / Eds.: Filippov N. B., Spiridonov M. A. Comilfo, 2009. 57 p.
27. Atlas of geological and geoecological maps of the Russian part of the Baltic Sea. / Ed. Petrov O. V. SPb.: VSEGEI, 2010. 78 p.
28. *Harff J., Meyer M.* Coastlines of the Baltic Sea – zones of competition between geological processes and a changing climate: Examples from the southern Baltic // J. Harff, S. Björck, P. Hoth, eds., The Baltic Sea Basin. Berlin, Heidelberg: Springer, 2011. P. 149—164.
29. *Гордеева С. М., Малинин В. Н.* Изменчивость морского уровня Финского залива. СПб.: РГГМУ, 2014. 179 с.
30. *Funkquist L.* HIROMB, an operational eddy-resolving model for the Baltic Sea // Bulletin of the Maritime Institute in Gdansk. 2001. V. 28, N 2. P. 7—16.
31. *Körnich H., Berggren L.* Joint WMO technical progress report on the global data processing and forecasting system and numerical weather prediction research activities for 2013. SMHI, 2013.
32. URL:https://www.wmo.int/pages/prog/www/DPFS/ProgressReports/2013/documents/2013_Sweden.doc (Дата обращения: 20.04.18).
33. *Hunt I. A.* Design of Seawalls and Breakwaters // J. of Waterway and Harbors Div. 1959. V. 85. P. 123—152.
34. *Sunamura T.* Sandy Beach Geomorphology Elucidated by Laboratory Modeling / Coastal Modeling: Techniques and Applications. Lakhan V. C., Trenhail A. S. (Eds). Elsevier, Amsterdam, 1989. P. 159—213.

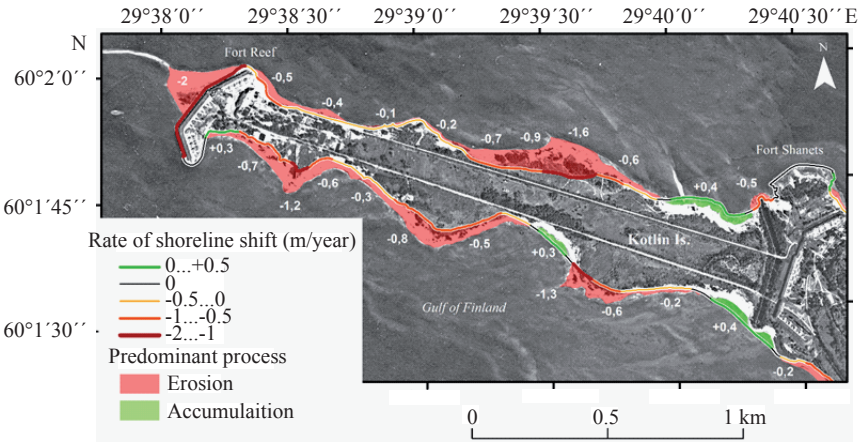

Fig. 1. The main features of coastal dynamics of the western KI.
The retrospective analysis was carried out using an air photo taken on 15.08.1939. The image with a resolution of 2 m is retrieved from the open access data set http://www.wwii-photos-maps.com. The recent coastline configuration is taken from the Yandex maps with a resolution of 1 m. The date of the image is 02.07.2015.

Рис. 1. Основные особенности прибрежной динамики западной части о. Котлин.
Ретроспективный анализ проводился с использованием аэрофотоснимка, сделанного 15.08.1939 г. Это изображение с разрешением 2 м извлекается из набора данных открытого доступа http://www.wwii-photos-maps.com. Последняя конфигурация береговой линии берется с карт Яндекса с разрешением 1 м. Дата изображения: 02.07.2015 г.

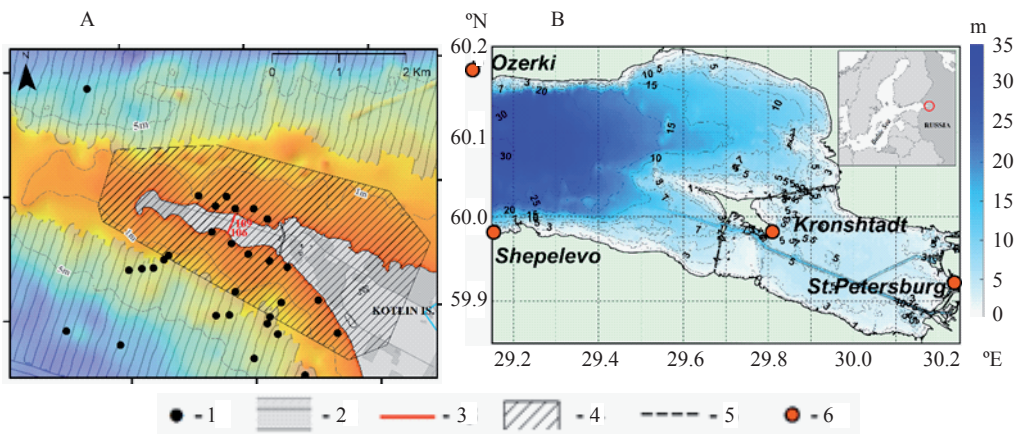

Fig. 2. The study area.
Panel A: map with location of: 1 — sediment sampling sites; 2 — side-scan sonar profiles; 3 — ground-penetrating radar profiles; 4 — area for which the remote sensing data were analysed; 5 — isobaths (m). Panel B: the model domain and bathymetry with locations of hydrometeorological stations (6). The insertion in the upper right corner: location of the study area in the Baltic Sea. Station “Ozerki” (60° 13' N, 29° 00' E) is located outside the model domain. The bathymetry was constructed based on field measurements conducted during the geological survey in 2016.

Рис. 2. Область исследования.
Фрагмент А: карта с расположением: 1 — участков отбора проб осадков; 2 — профилей гидролокаторов бокового обзора; 3 — профилей георадара; 4 — области, для которой были проанализированы данные дистанционного зондирования; 5 — изобат (м).
Фрагмент В: модельная область и батиметрия с местоположениями гидрометеорологических станций (6). Вставка в верхнем правом углу: место проведения исследования в Балтийском море. Станция «Озерки» (60°13'с.ш., 29°00'в.д.) находится за пределами модельного домена.
Батиметрия построена на основе полевых измерений, проведенных в ходе геологической съемки в 2016 г.

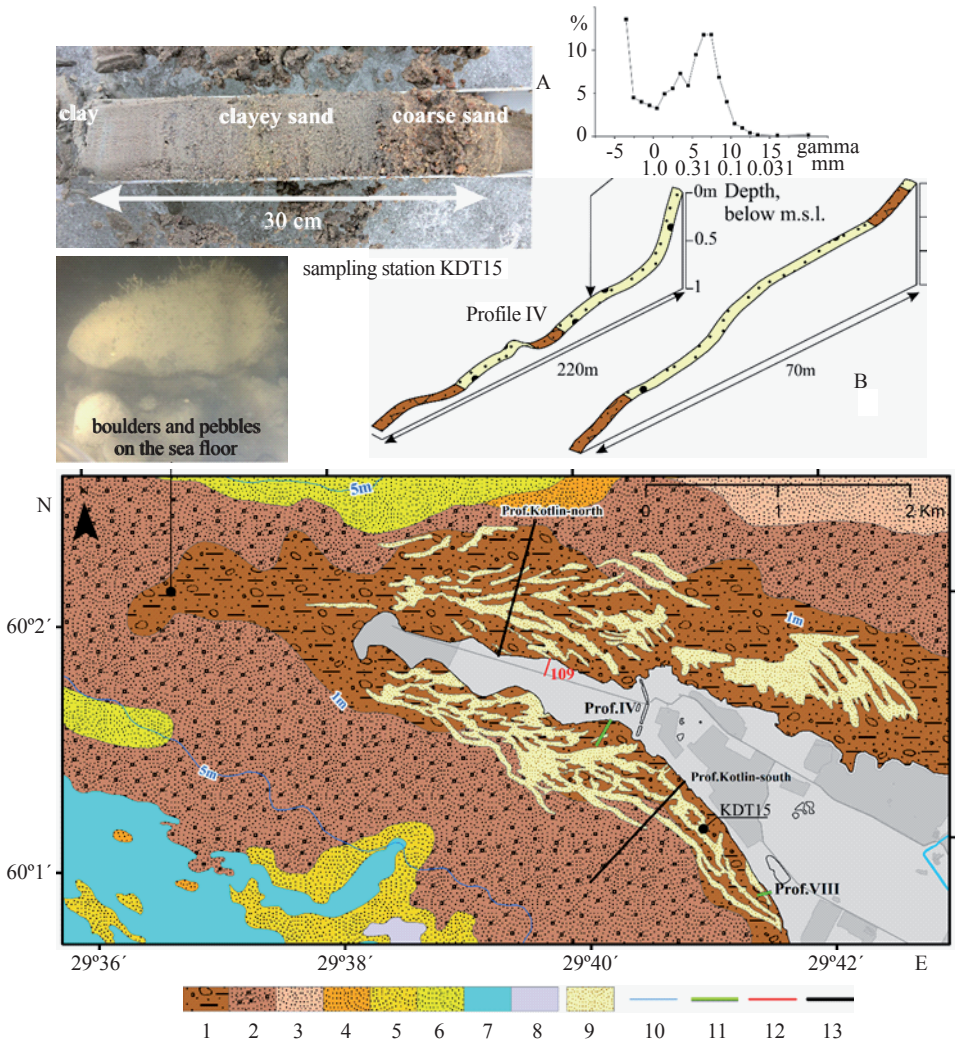

Fig. 4. The map of seabed of the nearshore of the western KI.

The legend describes the surface sediment types: 1 — boulders, pebbles, gravel; 2 — boulders, pebbles, gravel, sand; sand: 3 — unsorted, mainly coarse-grained; 4 — sand with gravel; 5 — coarse-grained sand; 6 — coarse- to medium grained sand; 7 — silt; 8 — sandy-silty-clayey mud; 9 — longshore sand ridges; 10 — isobaths; 11 — location of cross-shore sea-bed profiles; 12 — location of ground-penetrating radar profiles; 13 — location of profiles to be used in modelling. A — core of sediments from drilling site KDT-15; B — samples of cross-shore sea-bed profiles.

Рис. 4. Карта донных отложений прибрежной зоны западной части о. Котлин.

Описание типов поверхностных осадков: 1 — валуны, галька, гравий; 2 — валуны, галька, гравий, песок; песок: 3 — несортированный, преимущественно крупнозернистый; 4 — песок с гравием; 5 — крупнозернистый песок, 6 — крупно- и среднезернистый песок; 7 — ил; 8 — песчано-иловато-глинистая грязь; 9 — береговые песчаные гряды; 10 — изобаты; 11 — положение поперечных профилей морского дна; 12 — положение профилей георадара; 13 — положение профилей, используемых при моделировании. А — керн донных отложений станции КДТ15; В — примеры поперечных профилей подводного берегового склона.

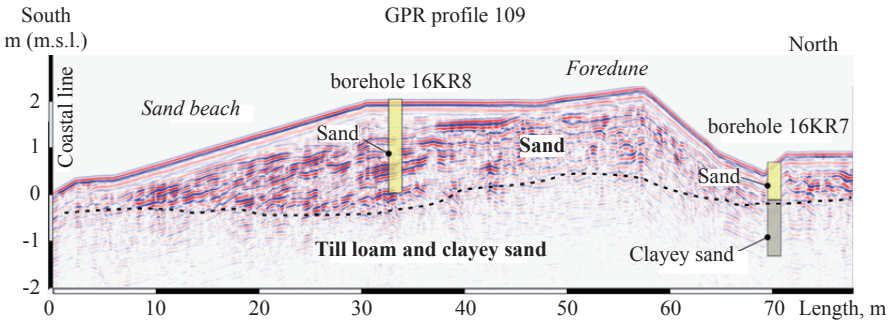

Fig. 5. A ground-penetrating radar image across the KI (GPR profile 109; see fig. 2 for the location of the profile).

Рис. 5. Изображение поперечного разреза острова Котлин, полученное с помощью георадара (профиль GPR 109, см. местоположение профиля на рис. 2).

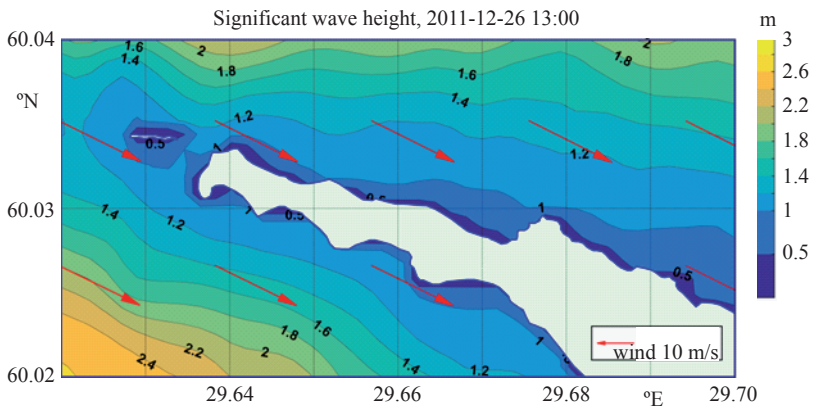

Fig. 9. The modelled SWH using the unadjusted HIRLAM wind speed on December 26.

Рис. 9. Рассчитанная значительная высота волн (ЗВВ) при использовании нескорректированной скорости ветра HIRLAM 26 декабря.

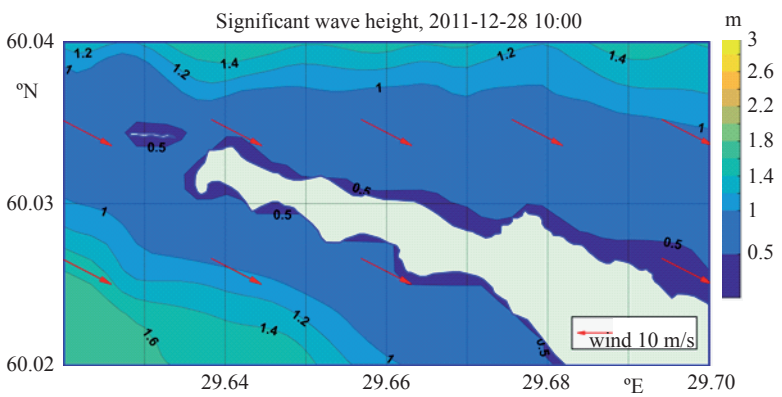

Fig. 10. The modelled SWH using the unadjusted HIRLAM wind speed on December 28.

Рис.10. Рассчитанная ЗВВ при использовании нескорректированной скорости ветра HIRLAM 28 декабря.